
FOURIERCSP: Differentiable Constraint Satisfaction Problem Solving by Walsh-Fourier Expansion

Yunuo Cen¹ Zixuan Wang¹ Jintao Zhang¹ Zhiwei Zhang² Xuanyao Fong¹

Abstract

The Constraint-Satisfaction Problem (CSP) is fundamental in mathematics, physics, and theoretical computer science. Continuous Local Search (CLS) solvers, as recent advancements, can achieve highly competitive results on certain classes of Boolean Satisfiability (SAT) problems. Motivated by these advances, we extend the CLS framework from Boolean SAT to general CSP with finite-domain variables and expressive constraint formulations. We present FOURIERCSP, a continuous optimization framework that generalizes the Walsh-Fourier transform to CSP, allowing for transforming versatile constraints to compact multilinear polynomials, thereby avoiding the need for auxiliary variables and memory-intensive encodings. We employ projected subgradient and mirror descent algorithms with provable convergence guarantees, and further combine them to accelerate gradient-based optimization. Empirical results on benchmark suites demonstrate that FOURIERCSP is scalable and competitive, significantly broadening the class of problems that can be efficiently solved by differentiable CLS techniques and paving the way toward end-to-end neurosymbolic integration.

1. Introduction

The Constraint-Satisfaction Problem (CSP) is foundational in mathematics, physics, and theoretical computer science. Formally, a CSP consists of variables defined over finite domains and a set of constraints restricting their values; the objective is to identify an assignment that satisfies all constraints. Applications of CSP solving span diverse fields, including artificial intelligence (Baluta et al., 2019), database query (Kolaitis & Vardi, 1998), operational research (Brails-

ford et al., 1999), statistical physics (Nagy et al., 2024), information theory (Golia et al., 2022), and quantum computing (Vardi & Zhang, 2022). Despite their significant importance, CSP inherently exhibits a combinatorial nature and is generally NP-complete, presenting a substantial challenge in solving it efficiently. Consequently, extensive research and development efforts have been dedicated to advancing CSP solving (Schulte et al., 2006; Hebrard, 2008; Kuchcinski & Szymanek, 2013; Prud’homme & Fages, 2022; Perron et al., 2023; Krupke et al., 2024).

Although classical CSP engines (Schulte et al., 2006; Hebrard, 2008; Kuchcinski & Szymanek, 2013; Prud’homme & Fages, 2022) are powerful, their reliance on backtracking and discrete propagation creates a fundamental barrier for deep learning integration. The lack of differentiability precludes backpropagation, hindering the embedding of constraint reasoning into neural architectures. Recent hybrid approaches have attempted to bridge this gap by learning heuristics for branching and cut selection (Khalil et al., 2016; Zhang et al., 2022; Ling et al., 2024; Vo et al., 2025; Zeng et al., 2025; Gasse et al., 2019). However, these methods merely augment the discrete search process and do not yield differentiable solvers.

In parallel, Continuous Local Search (CLS) approaches for Boolean Satisfiability (SAT) have demonstrated that gradient-based optimization on smooth multilinear relaxations can yield highly effective differentiable solvers (Kyrillidis et al., 2020; 2021b). Yet, these formulations rely on the algebraic properties of Boolean variables $\{\pm 1\}$, making them inapplicable to the multi-valued domains and rich constraints found in general CSPs. Existing differentiable CSP techniques generally rely on ad-hoc heuristics or specific constraint types (Xu et al., 2018; Goyal et al., 2024; Xu et al., 2025), lacking a unified formulation for general finite-domain constraints.

This gap necessitates a differentiable framework that: (i) operates directly on finite-domain variables, avoiding the dimensionality explosion of Boolean encodings; (ii) can formulate versatile constraints; and (iii) ensures the continuous relaxation faithfully captures the structure of the discrete feasibility region. To achieve this, we utilize the Walsh-Fourier basis, which provides an orthogonal multilin-

¹Department of Electrical and Computer Engineering, National University of Singapore, Singapore ²Department of Computer Science, Rice University, Houston, Texas, United States. Correspondence to: Xuanyao Fong <kelvin.xy.fong@nus.edu.sg>.

ear expansion that yields smooth optimization landscapes, ideal for projected subgradient and mirror-descent methods. While Fourier-based relaxations have proven effective for Boolean SAT (Kyrillidis et al., 2020; 2021b), in this work, we generalize the Walsh-Fourier transform to the finite-domain setting. This provides a principled algebraic foundation for differentiable CSP solving, extending the capabilities of CLS beyond the Boolean domain. The contribution of this paper can be summarized as follows:

A Uniform Differentiable CSP Framework: We provide a rigorous algebraic generalization of the Walsh-Fourier transform for variables with finite domains. The proposed framework is called FOURIERCSP. It established a principled basis for differentiable constraint solving.

Provable Optimization Algorithm: In addition to the FOURIERCSP framework, we develop specialized variants of projected subgradient and mirror-descent methods tailored to this setting. We provide rigorous convergence guarantees, ensuring the reliability of the continuous search.

Efficient Implementation and Empirical Evaluation: We conduct extensive evaluations on standard benchmark suites. Our results demonstrate that FOURIERCSP is highly scalable and competitive with existing baselines, significantly broadening the scope of problems solvable by differentiable techniques.

2. Preliminaries

Constraint Satisfaction Problem Let $X = \{x_1, \dots, x_n\}$ be a set of variables, and $D = \{\text{dom}(x_1), \dots, \text{dom}(x_n)\}$ be a set of finite domains, and $C = \{c_1, \dots, c_m\}$ be a set of constraints. Every constraint $c_i \in C$ is described by an atom set $A_i \subseteq X$. The (finite-domain) CSP is to find an assignment of X over D such that a finite-domain formula, *i.e.*, the conjunction of all constraints, $F = \bigwedge_{c_i \in C} c_i$, is satisfiable.

Walsh-Fourier Transform We define a function with finite domain by $f : D \rightarrow \{0, 1\}$, where 0 and 1 present false, true of the finite constraint.

The Walsh-Fourier Transform is a method for transforming a function with a finite domain into a multilinear polynomial. Given the Fourier bases, any function defined on a finite domain has an equivalent Fourier representation.

Definition 2.1 (Fourier Bases). Given a function on a finite domain $f : D \rightarrow \{0, 1\}$, we define the Fourier bases ϕ_α by

$$\phi_\alpha(X) = \prod_{i=1}^n \phi_{\alpha_i}(x_i),$$

where $\alpha_i \in \text{dom}(x_i)$, and ϕ_{α_i} is an indicator basis, *i.e.*, $\phi_{\alpha_i}(x_i)$ equals to 1 if $\alpha_i = x_i$, otherwise equals to 0.

Theorem 2.2 (Walsh-Fourier Expansion (O’Donnell, 2014)). *Having fixed the Fourier bases, f is uniquely expressible as*

$$f(X) = \sum_{\alpha \in D} \left(\hat{f}(\alpha) \cdot \phi_\alpha(X) \right)$$

where $\hat{f}(\alpha) \in \mathbb{R}$ is called Fourier coefficient, and it satisfies

$$\hat{f}(\alpha) = \mathbb{E}_{X \sim D} [f(X) \cdot \phi_\alpha(X)].$$

3. Theoretical Framework

In this section, we first recap the previous CLS for Boolean SAT solving. We then demonstrate how our proposed solver, FOURIERCSP, can extend the CLS framework to general constraint satisfaction problems. Proofs are delayed to Appendix A.

3.1. Continuous Local Search

CLS-based solvers define a continuous objective function, the optima of which encode the solutions to the original problem defined on discrete variables. The CLS approach for SAT solving was initially proposed in UNISAT (Gu, 1994). Modern variants, like FOURIERSAT (Kyrillidis et al., 2020), GRADSAT (Kyrillidis et al., 2021b) transform Boolean constraints to continuous functions, called Walsh-Fourier Expansion (WFE) via the Walsh-Fourier transform (O’Donnell, 2014). FASTFOURIERSAT is the parallel version of FOURIERSAT and achieve more than 100× speedup in gradient computation (Cen et al., 2025). These approaches solve the following objective, and the algorithmic framework is described in Algorithm 1.

Definition 3.1 (Objective). Given a formula $F = \bigwedge_{c \in C} c$, every constraint $c \in C$ can be transformed to a function by Theorem 2.2. We denote the corresponding expansion as f_c and the objective function w.r.t. F by

$$\mathcal{F} = - \sum_{c \in C} f_c.$$

The entire lineage of CLS solvers, from the 1990s approaches (Gu, 1994) to modern variants, is exclusively designed for Boolean constraints. While they perform well on certain problem classes, these solvers often fail to scale effectively to large or complex CSP instances. This limitation becomes particularly acute for finite-domain problems, which require conversion to potentially larger Boolean formulas. This limitation fundamentally restricts their practical application for real-world problems that naturally require finite-domain representations.

3.2. FourierCSP

To address the above limitation, we propose FOURIERCSP, a CLS framework that directly supports finite-domain CSPs

Algorithm 1 Continuous Local Search

Input: A formula F with a constraint set C
Output: A discrete assignment $X \in D$

- 1: Sample P from \tilde{D}
- 2: **for** $j = 1, \dots, \text{max_iter}$ **do**
- 3: Search for a local optimum P^* of $\mathcal{F}(P)$
- 4: Discretized assignment: $X = \mathcal{R}(P^*)$
- 5: **if** $\mathcal{F}(X) = -|C|$ **then**
- 6: **return** X
- 7: **end if**
- 8: **end for**
- 9: **return** X with the highest $\mathcal{F}(X)$

without requiring Booleanization. We start by applying randomized rounding to the generalized form of WFE in Theorem 2.2, which reduces the CSP to a differentiable multilinear function over a product of probability simplices. In particular, although stationary points may occur in the interior of the domain, we prove that *every local minimum of the multilinear objective must lie on the boundary* of the simplices, ensuring the solution quality. Building on this differentiable formulation, we analyze the behavior of Projected Gradient Descent (PGD) and Mirror Descent (MD) and derive practical convergence bounds for both methods. Based on these theoretical insights, we propose a Hybrid Descent (HD) that combines PGD and MD, exploiting their complementary geometries to accelerate convergence.

Reduction by Randomized Rounding Theorem 2.2 illustrates how to expand discrete functions to multilinear polynomials through WFE. The resulting Fourier coefficients $\hat{f}(\alpha)$ provide valuable insights into analyzing the discrete function properties. However, the expanded function f remains discrete and non-differentiable given the Fourier Bases in Definition 2.1, limiting its utility for gradient-based optimization. To enable continuous optimization, we introduce a randomized rounding \mathcal{R} that relaxes discrete variable assignments into a continuous domain. Consider a set of finite domain variables $X = \{x_1, \dots, x_n\}$. The vector probability space of x_i is a simplex denoted by

$$\tilde{D}_i := \left\{ p_{i,j} \mid \min_{j \in \text{dom}(x_i)} p_{i,j} \geq 0, \sum_{j \in \text{dom}(x_i)} p_{i,j} = 1 \right\}.$$

The collection of all simplexes forms a continuous search space $\tilde{D} = (\tilde{D}_1 \times \dots \times \tilde{D}_n)$.

Definition 3.2 (Randomized Rounding). Given a finite domain D . The randomized rounding function, denoted by $\mathcal{R} : \tilde{D} \rightarrow D$ is defined by

$$\mathbb{P}[\mathcal{R}(P)_i = j] = p_{i,j}$$

for all $j \in \text{dom}(x_i)$, $p_i \in \tilde{D}_i$ and $i \in [n]$.

Intuitively, if $p_{i,j}$ is closer to 1, then $\mathcal{R}(a)_i$ is more likely to be rounded to j . Using this randomized interpretation, we can define a probability distribution over full assignments by rounding \mathcal{R} of each variable independently.

Definition 3.3 (Probability Space). We define a probability space on a discrete matrix w.r.t. to real point $P \in \tilde{D}$, denoted by $\mathcal{S} : D \rightarrow [0, 1]$, as:

$$\mathcal{S}_P(X) = \mathbb{P}[\mathcal{R}(P) = X] = \prod_{i=1}^n p_{i,x_i},$$

for all $X \in D$, with respect to the randomized-rounding function \mathcal{R} . We use $X \sim \mathcal{S}_P$ to denote that X is sampled from the probability space \mathcal{S}_P .

The probability space allows us to define a continuous extension of any discrete function by taking its expectation over a randomized assignment.

Theorem 3.4 (Expectation). *Given a Walsh-Fourier expansion \mathcal{F} , for a real point $P \in \tilde{D}$, we have*

$$\begin{aligned} \mathbb{E}_{X \sim \mathcal{S}_P} [\mathcal{F}(X)] &= \mathbb{E}_{X \sim \mathcal{S}_P} \left[- \sum_{c \in C} f_c(X) \right] \\ &= - \sum_{c \in C} \sum_{\alpha} \left(\hat{f}_c(\alpha) \cdot \prod_{i=1}^n p_{i,\alpha_i} \right) \quad (1) \\ &= \mathcal{F}(P). \end{aligned}$$

We can observe from Theorem 3.4 that $\mathcal{F}(P)$ is a multilinear polynomial. Therefore, we relax the domain from discrete D to continuous \tilde{D} , and it leads to a ρ -Lipschitz, and L -smooth multilinear continuous function.

Proposition 3.5 (Lipschitz). *Let $\mathcal{F} : \tilde{D} \rightarrow [-|C|, 0]$ be a multilinear polynomial. Let n be the number of variable, then $N = \sum_{i=1}^n |\text{dom}(x_i)|$. For every point $P, P' \in \tilde{D}$, we have*

$$\begin{aligned} |\mathcal{F}(P) - \mathcal{F}(P')| &\leq \rho \|P - P'\|, \\ |\nabla \mathcal{F}(P) - \nabla \mathcal{F}(P')| &\leq L \|P - P'\|, \end{aligned}$$

where $\rho = |C|N^{\frac{1}{2}}$, $L = |C|N$.

As the expectation is a continuous and smooth multilinear polynomial, we formalize the reduction in Theorem 3.6.

Theorem 3.6 (Reduction). *Given a constraint satisfaction problem of formula F , which is the conjunction of all constraints $c \in C$. F is satisfiable if and only if*

$$\min_{P \in \tilde{D}} \left(\mathbb{E}_{X \sim \mathcal{S}_P} [\mathcal{F}(X)] \right) = -|C|. \quad (2)$$

3.3. Optimization Approaches

The essence of CLS is using continuous optimization to find the minima of a non-convex but smooth function, where the

smoothness of the WFE was analyzed in Proposition 3.5. Given the inherent difficulty of optimizing non-convex functions (Jain & Kar, 2017), it is often sufficient in practice to converge to a local optimum and subsequently verify, via Theorem 3.6, whether it corresponds to a global solution. During continuous optimization, the descent steps move the assignment toward regions of lower objective value, and the iterate eventually reaches a local minimum at which the suboptimality gap $\mathcal{F}(P_t) - \mathcal{F}(P^*)$ becomes small, typically $\leq \epsilon$. A potential concern is the existence of local minima strictly inside the feasible region, *i.e.*, in $\tilde{D} \setminus \delta\tilde{D}$, since such points would provide no guarantee about the quality of the decoded discrete assignment. However, Lemma 3.7 establishes that no interior local maxima exist for our multilinear objective, and thus all optimal points lie on the boundary. This structural property directly leads to Theorem 3.8.

Lemma 3.7. *Let \tilde{D}_\perp be a hyperplane with $\vec{1}$ as the normal vector. For every non-constant \mathcal{F} and a point $P \in \tilde{D} \setminus \delta\tilde{D}$, there exist a region size $\epsilon > 0$ and a directions, $V \in \tilde{D}_\perp$ such that for all $\eta \in (0, \epsilon)$, the following holds.*

$$\mathcal{F}(P - \eta V) < \mathcal{F}(P)$$

Theorem 3.8 (Optimality). *Any interior point $P \in \tilde{D} \setminus \delta\tilde{D}$ cannot be a local optimum of $\mathcal{F}(P)$. The optimal points are only attained from the boundary $\delta\tilde{D}$.*

Having established these optimization characteristics, the next question is how different descent geometries behave within this landscape. In particular, PGD and MD offer distinct update rules and induce different optimization geometries on the probability simplices.

Projected Gradient Descent Since Eq. (1) is defined only over the constrained domain \tilde{D} , a single gradient step may result in an intermediate point that falls outside this domain. Therefore, each gradient step, *i.e.*, Eq. (3), must be followed by a projection, *i.e.*, Eq. (4), back onto \tilde{D} to ensure feasibility.

$$Q_{t+1} = P_t - \eta \cdot \nabla \mathcal{F}(P_t) \quad (3)$$

$$P_{t+1} = \text{proj}_{\tilde{D}}(Q_{t+1}) \quad (4)$$

Based on the randomized rounding in Definition 3.2, the Euclidean projection of $Q \in \mathbb{R}^{|\text{dom}(x_1)| \times \dots \times |\text{dom}(x_n)|}$, onto $P \in \tilde{D}$, is defined as

$$\text{proj}_{\tilde{D}}(Q) = \arg \min_P \left(I_{\tilde{D}}(P) + \frac{1}{2} \|Q - P\|_2^2 \right), \quad (5)$$

where $I_{\tilde{D}}$ is an indication function. $I_{\tilde{D}}(P)$ is ∞ (resp. 0) when $P \notin \tilde{D}$ (resp. \in).

The projection operation $\text{proj}_{\tilde{D}}(Q)$ can be computed efficiently by separately projecting each q_i onto its respective

simplex \tilde{D}_i , leveraging the product structure of \tilde{D} . Each sub-projection corresponds to a standard simplex projection problem (Chen & Ye, 2011).

Theorem 3.9. *With the step size $\eta = \frac{1}{L}$, the PGD will converge to a ϵ -critical point in $\mathcal{O}\left(\frac{|C| \cdot L}{\epsilon^2}\right)$ iterations.*

Mirror Descent While projected gradient methods rely on Euclidean geometry for projection, MD generalizes this process to non-Euclidean geometries induced by a strictly convex potential function ψ .

$$\begin{aligned} Q_{t+1} &= \nabla \psi(P_t) - \eta \nabla \mathcal{F}(P_t), \\ P_{t+1} &= \nabla \psi^{-1}(Q_{t+1}). \end{aligned}$$

We choose negative entropy as the potential function for each probability simplex \tilde{D}_i , hence $\psi(P) = \langle P, \log(P) \rangle$. Then we have

$$\nabla \psi(P) = \log(P), \quad \nabla \psi^{-1}(Q) = \frac{\exp(Q)}{\langle \exp(Q), \mathbf{1} \rangle}.$$

Theorem 3.10. *Let $\Theta = \sum_{i=1}^n \log |\text{dom}(x_i)|$. Let T be the number of MD steps. with the step size $\eta \leq \frac{\sqrt{2\Theta}}{\rho\sqrt{T}}$, then MD will converge to a ϵ -critical point in $\mathcal{O}\left(\frac{2\Theta \cdot \rho}{\epsilon^2}\right)$ iterations.*

Hybrid Descent Theorem 3.9 implies a larger gradient norm $\|\nabla \mathcal{F}\|$ leads to a greater decrease in the objective at each projected gradient step, and therefore accelerates convergence. In contrast, Theorem 3.10 requires a global bound $\|\nabla \mathcal{F}\| \leq \rho$, and a larger gradient increases this bound, which forces a smaller step-size in the analysis and ultimately slows the convergence rate of MD. This contrast is made explicit in (Allen-Zhu & Orecchia, 2014), which shows that PGD and MD operate under different geometries and therefore complement each other. Motivated by this observation, we adopt a hybrid update rule, HD, that evaluates both descent directions and selects the better one:

$$\begin{aligned} P_{PGD} &= \text{proj}_{\tilde{D}}(P_t - \eta_{PGD} \cdot \nabla \mathcal{F}(P_t)), \\ P_{MD} &= \nabla \psi^{-1}(\nabla \psi(P_t) - \eta_{MD} \nabla \mathcal{F}(P_t)), \\ P_{t+1} &= \arg \min_{P \in \{P_{PGD}, P_{MD}\}} \mathcal{F}(P). \end{aligned}$$

Implementation Details FOURIERCSP is implemented by extending the core JAXOPT.PROJECTEDGRADIENT framework and incorporating the projection and mapping functions from JAXOPT.MIRRORDESCENT (Bradbury et al., 2018; Blondel et al., 2022). We adopt the default settings in JAXOPT, using a maximum of 500 gradient steps and a tolerance of 0.001. The step size is determined automatically via backtracking line search, with a maximum of 15 backtracking steps and a decrease factor of 0.5. All descent methods are evaluated both with and without Fast Iterative Shrinkage-Thresholding Algorithm (FISTA) acceleration.

4. Experimental Section

In this section, we compare our tool, FOURIERCSP, with versatile state-of-the-art solvers. The objective of our experiments is to answer the following research questions.

RQ1. Given their Boolean-encoded formulas of CSP, how well does FOURIERCSP perform in solving them?

RQ2. How do different descent methods compare in effectiveness and robustness in the FOURIERCSP framework?

RQ3. How does FOURIERCSP compare to SAT, ILP, and CP solvers in solving constraint satisfaction problems that the constraints have structural patterns?

RQ4. How does FOURIERCSP perform relative to SAT, ILP, and CP solvers in solving constraint optimization problems that the constraints have structural patterns?

Benchmarks and Encodings To fully exploit the potential of Fourier expansion-based CLS, benchmark instances should ideally be symmetric, *i.e.*, their constraints should exhibit similar structural patterns. This symmetry enables efficient GPU acceleration by allowing the solver to fully utilize parallelism, achieving up to 100+ times speedup in gradient computation compared to CPU (Cen et al., 2025). The benchmarks include constraint satisfaction and optimization problems. The first benchmark consists of **random hybrid constraints**, combining *greater-than*, *not-all-equal*, and *modulo* constraints. For each combination of $n_{\text{var}} \in \{100, \dots, 1000\}$ and $n_{\text{state}} \in \{4, 8, 16, 32\}$, we generate 10 random instances. Each instance contains $\frac{n_{\text{var}}}{10}$ of each type. The arity (length) of NAE and modulo constraints is fixed to 10. The second benchmark is **task scheduling problems**, which can be useful for the trace scheduler of multicore hardware systems. For each combination of $N_{\text{worker}} \in \{32, 64, 128, 256, 512\}$ and $m \in \{4, 8, 16\}$, we set the number of jobs to $N_{\text{job}} = m \cdot N_{\text{worker}}$, and generate 10 random instances accordingly. The third benchmark, **graph coloring with hashing queries**, is an optimization problem motivated by approximate model counting (Pote et al., 2025), where hash functions are employed to partition the solution space. We use graph coloring as the underlying problem and add parity (modulo 2) constraints to the formula to serve as hash functions. For each $N_{\text{node}} \in \{512, 1024, 2048, 4096\}$ and $N_{\text{color}} \in \{8, 16, 32, 64\}$, we generate 10 random instances. Additionally, N_{node} modulo 2 constraints are added to each instance.

Benchmark instances are linearized for ILP solvers and Booleanized for Boolean SAT solvers. Further details on the benchmarks and the encodings used for different solvers can be found in the appendix, where we show that the Booleanization will naturally lead to pseudo-Boolean and XOR constraints. Further encoding the largest Booleanized instance into CNF (Ignatiev et al., 2018; Li, 2000) yields

a formula comprising over 160 million variables and 710 million clauses. Although modern SAT solvers are highly optimized and capable of solving large benchmarks, such encodings are extremely memory-inefficient; for instance, the corresponding CNF text file is around 16 GB in size. The details of the encoding are in Appendix B.

Solver Competitors (1) **FOURIERSAT** (Kyrillidis et al., 2020): A CLS solver designed for Boolean formulas that are conjunctions of symmetric Boolean constraints. In (Cen et al., 2025), it uses PGD with FISTA as the optimizer. (2) **FOURIERMAXSAT** (Cen et al., 2025): An extension of FourierSAT incorporating an SAT solver for warm-start initialization. (3) **LINPB** (Yang & Meel, 2021): A SAT solver for linear pseudo-Boolean and XOR constraints. It employs RoundingSAT, which extends CDCL to pseudo-Boolean reasoning, as the underlying pseudo-Boolean solver. XOR constraints are supported via Gauss-Jordan elimination, adapted from CryptoMiniSAT. (4) **GUROBI-ILP** (Gurobi Optimization, LLC, 2024): An ILP solver that uses branch-and-bound, cutting planes, and heuristics to handle integer linear constraints efficiently. The solver also leverages preprocessing and parallel computation to enhance performance. We use version 11.0.3. (5) **OR-TOOLS CP-SAT** (Perron et al., 2023): A hybrid solver that integrates a clause-learning SAT core, constraint programming, and linear relaxation within a unified model to solve combinatorial problems using advanced techniques; it won gold medals in all categories of the MiniZinc Challenge 2024. This solver won gold medals in all categories in the MiniZinc Challenge 2024. We use version 9.11. (6) **PARAILP** (Lin et al., 2024): A parallel discrete local search solver for ILP.

Experimental Setups Solvers run on a high-performance cluster node with dual AMD EPYC 9654 CPUs, 24×96 GB DRAM, and 8 NVIDIA L40S GPUs. We allow GUROBI-ILP, OR-TOOLS CP-SAT, and PARAILP to use maximally 256 threads. As SAT solvers are particularly memory-intensive due to clause database management (Alekhovich et al., 2000; Elffers et al., 2016), simple parallelization via multi-threaded racing, without inter-thread clause sharing, typically yields limited performance improvements. Consequently, LINPB, which does not support multithreading, is executed in single-threaded mode. The CLS solvers, FOURIERSAT and FOURIERCSP, are executed on the GPU to exploit their inherent parallelism and leverage the computational advantages of modern GPU architectures. We set 1000 seconds as the timeout for each instance.

We assess solver performance on satisfaction problems using the PAR-2 (penalized average runtime 2) score, a metric balancing runtime efficiency and robustness by imposing

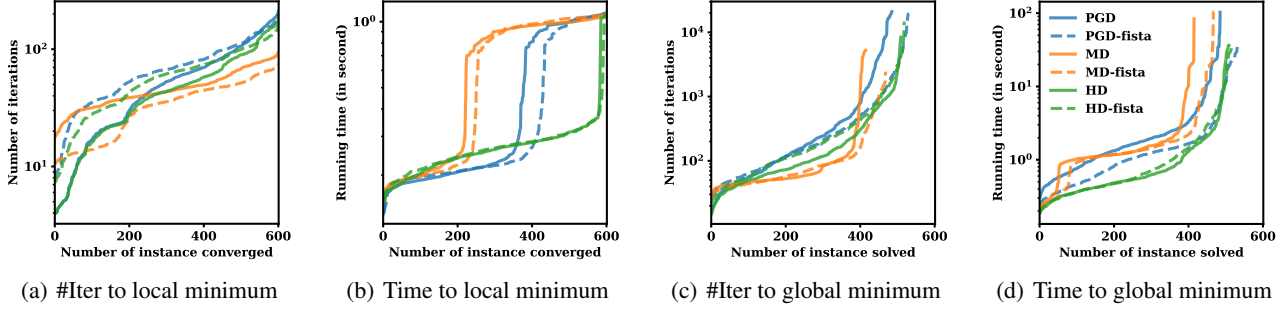


Figure 1. The performance of FOURIERCSP with different descent methods on the random benchmark.

penalties on timeouts.

$$\text{PAR-2} = \frac{1}{N} \sum_{i=1}^N (t_i \cdot \mathbf{1}[t_i \leq T] + 2T \cdot \mathbf{1}[t_i > T])$$

where $\mathbf{1}(\cdot)$ is the indicator function and T is the time limit.

We evaluate the optimization problem using two metrics: the relative score and the number of instances for which a solver attains the best objective value (#Win). The relative score is defined as follows.

$$\text{score}(s, i) = \frac{1 + c_i^s}{1 + c_i^*}$$

where c_i^s denotes the result obtained for instance i by algorithm s , and c_i^* denotes the best-known result.

4.1. Answer to RQ1.

Since FOURIERCSP is the multi-valued extension of FOURIERSAT, the semantics of solving hybrid SAT formulas remain equivalent to those of FOURIERSAT. Prior research indicates that FOURIERSAT demonstrates strong performance on benchmarks natively formulated as hybrid SAT problems. However, our experiments reveal a significant limitation: FOURIERSAT fails to solve any instances encoded from both scheduling (Fig. 2) and graph coloring benchmarks (Fig. 3). This observation underscores a critical gap in the capability of FOURIERSAT when handling problems not inherently structured as conjunctions of symmetric Boolean constraints. Consequently, it highlights the necessity of extending the solver to a more general domain. Specifically, the results motivate the development of FOURIERCSP, a multi-valued extension of FOURIERSAT, which is designed to address these limitations precisely by supporting more general, *i.e.*, multi-valued formulations.

4.2. Answer to RQ2.

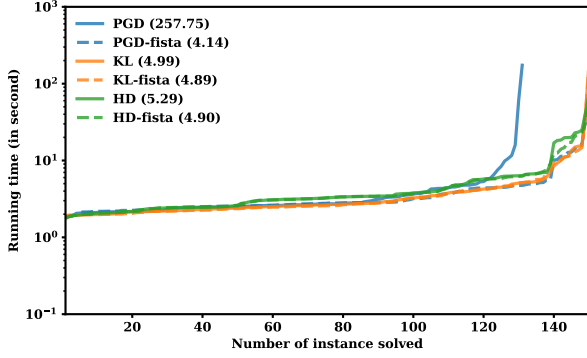
From Fig. 1 (a), MD requires the fewest gradient iterations to reach a local minimum. However, Fig. 1 (b) shows that

it nevertheless takes longer in wall-clock time. This is because all methods use line search to select the step size: although MD makes rapid progress per gradient step, its updates satisfy the line-search conditions less easily, causing more backtracking. As a result, each MD iteration is more expensive, leading to a higher total runtime despite fewer iterations. It’s counterintuitive that HD is the most time-efficient approach, where each gradient step needs to measure the gradient step made by both PGD and MD. This is because HD inherits the faster descent direction of the two while avoiding the costly backtracking behavior that slows down pure MD. The same pattern appears in Fig. 1(c–d) for convergence to the global minimum.

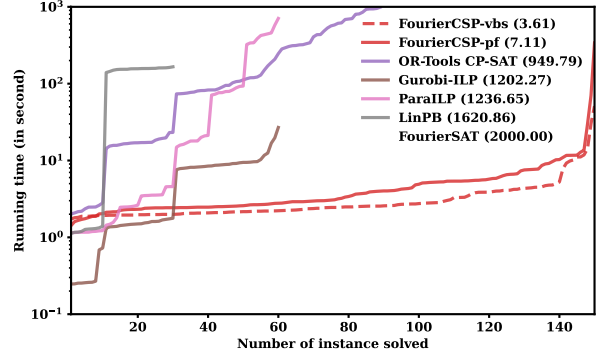
Across all settings, HD is the most effective and robust method within the FOURIERCSP framework for constraint satisfaction problems, consistently solving the largest number of instances under a fixed trial budget. FISTA further accelerates both PGD and MD, with PGD-fista performing competitively with HD and HD-fista. This trend is confirmed on the scheduling benchmark in Fig. 2 (a), where plain PGD is significantly slower than all other descent methods, while PGD-fista eliminates most of this gap, and even achieves the lowest PAR-2 score.

The results for the constraint optimization benchmark are reported in Table 1. Although PGD-fista achieves the highest anytime score, MD-fista yields the largest number of best solutions. Moreover, other descent methods also achieve the best result on certain instances, indicating that no single method uniformly dominates across all problems. These observations suggest that a portfolio strategy combining multiple descent methods is more reliable and robust than relying on any individual optimizer.

In the remainder of the paper, FOURIERCSP-vbs denotes the virtual-best solver across all descent variants, *i.e.*, a setting that evaluates each descent method in parallel using multiple GPUs. In contrast, FOURIERCSP-pf refers to a sequential portfolio strategy that runs all descent methods on a single GPU. As illustrated in Fig. 2(b), although FOURIERCSP-vbs employs 6 GPUs, its speedup over the



(a) FOURIERCSP with different descent methods.



(b) Comparison of FOURIERCSP with other solvers.

Figure 2. Results on task scheduling problems. The numbers in the legend are the average PAR-2 score of the solvers.

Descent Method	Anytime Score	#Win
PGD	0.87	26
PGD-fista	0.97	15
MD	0.80	20
MD-fista	0.76	46
HD	0.86	11
HD-fista	0.92	13

Table 1. Performance of FOURIERCSP with different descent methods on the graph coloring with hashing query benchmark.

single-GPU portfolio FOURIERCSP-pf remains below $2\times$. This phenomenon reflects a natural boundary effect: the fine-grained parallelism available within each constraint’s WFE evaluation is already saturated by a single GPU, leaving limited room for further acceleration. Additional GPUs mainly enable evaluating multiple random initializations with different descent methods concurrently, which improves robustness but cannot provide unbounded speedup.

4.3. Answer to RQ3.

Fig. 2 presents the results on the second benchmark, constraint satisfaction problems. FOURIERCSP and PARAILP represent two parallel local search solvers based on continuous and discrete optimization methods, respectively. Under a timeout limit of 1000 seconds, FOURIERCSP successfully solves all 150 instances, substantially surpassing PARAILP, which solves only 60. This significant performance gap can be attributed to the differences in the local search methods. Discrete local search methods require that each assignment strictly increase the number of satisfied constraints, often leading to plateaus, particularly for constraints that are long or structurally complex, where small perturbations to discrete variable assignments may not immediately yield progress. In contrast, CLS methods can exploit fine-grained improvements: the optimizer advances as long as the con-

tinuous objective decreases, even marginally.

Among complete solvers, OR-TOOLS CP-SAT, GUROBI-ILP, and LinPB solve 89, 60, and 30 instances, respectively. Although OR-TOOLS CP-SAT supports channeling constraints, it requires auxiliary variables for modeling conditional logic (*e.g.*, if-then-else), which can substantially expand the search space. A key advantage of FOURIERCSP is that it evaluates the Walsh-Fourier expansion directly, without introducing auxiliary variables, thus maintaining a lower-dimensional search space and preserving problem structure. As a result, FOURIERCSP-pf achieves a $133.59\times$ speedup in PAR-2 score compared to OR-TOOLS CP-SAT.

Instances solved by the ILP solvers are generated with $N_{\text{worker}} \leq 256$, and the resulting ILP formulas contain fewer than 130,000 variables and 162,000 linear constraints. Although PARAILP is an incomplete ILP solver, typically known for its efficiency in finding feasible solutions, *i.e.*, it underperforms GUROBI-ILP, as reflected by its higher PAR-2 score. Instances solved by LinPB are generated with $N_{\text{worker}} \leq 128$, where the encoded PB-XOR formulas contain fewer than 65,000 Boolean variables and 75,000 constraints. Despite its reasoning capabilities, LinPB must handle much larger formulas in practice: problems with $N_{\text{worker}} \leq 128$ result in formulas with approximately 295,000 variables and 325,000 constraints. FOURIERCSP-pf achieves a $169.10\times$ and $227.97\times$ speedup compared to GUROBI-ILP and LINPB, respectively. These results suggest that when solving CSP involving non-Boolean variables and non-linear constraints, a solver that can process more compact formulas, *i.e.*, without bloating the search space, can offer significant performance advantages.

4.4. Answer to RQ4.

This benchmark includes a substantial number of modulo constraints, which are known to be challenging for OR-TOOLS CP-SAT (Krupke et al., 2024). While modulo con-

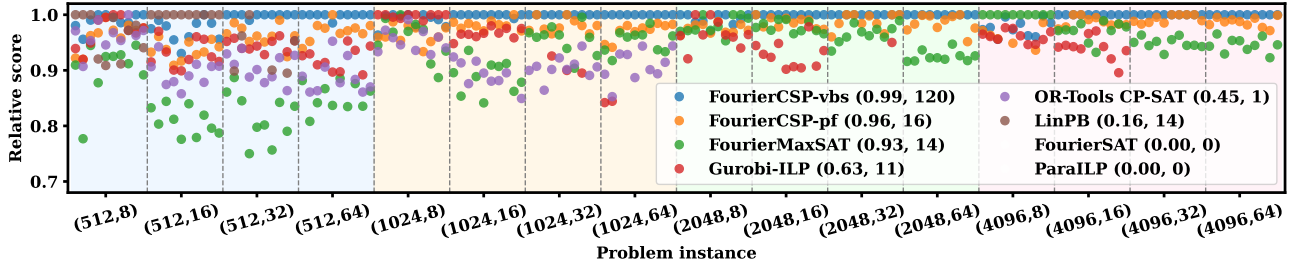


Figure 3. Results on graph coloring with hashing query problems. The numbers in the legend are (the average relative score, #Win) of the solvers.

straints remain beyond the expressive or algorithmic reach of most conventional solvers, FOURIERCSP can natively accommodate them through its uniform Fourier expansion framework. As shown in Fig. 3, FOURIERCSP-pf outperforms all competing solvers on this benchmark, achieving a relative score of 0.96. The FOURIERCSP-vbs setting reflects the performance upper bound of FOURIERCSP-pf and attains the best solution on 120 out of 160 instances. In contrast to its competitive performance on the previous benchmark, OR-TOOLS CP-SAT’s relative score is 0.18 lower than that of GUROBI-ILP for these instances. This relative underperformance can likely be attributed to OR-TOOLS CP-SAT’s inefficiency in processing modulo constraints.

Under binary logarithm encoding, a modulo 2 constraint can be easily Booleanized to an XOR constraint. Although LINPB can natively solve XOR constraints using Gaussian elimination, it achieves a relative score of 0.16 on this benchmark. Nevertheless, LINPB contributes more to the virtual best solver than OR-TOOLS CP-SAT, as it attains the best solution for 14 instances. Notably, formulas with parity constraints are known to be challenging for DLS solvers (Crawford et al., 1994). Unsurprisingly, PARAILP fails to provide valid solutions for any instance in this benchmark.

Previous work demonstrated that FOURIERSAT performs competitively on graph problems when the encoded formulas comprise exclusively symmetric Boolean constraints (Cen et al., 2025). In contrast, the Booleanized formulas used in this benchmark consist primarily of pseudo-Boolean constraints, which would require further symmetrization into disjunctive clauses to fit the FOURIERSAT framework. This additional encoding step increases the complexity, making the problem significantly more challenging for FOURIERSAT, which does not provide valid solutions for any instance in this benchmark. While FOURIERSAT encounters difficulties when addressing formulas containing a large number of clauses, FOURIERMAXSAT adopts a hybrid approach. It leverages a SAT solver to solve part of the formula, *i.e.*, the disjunctive clauses, and subsequently uses CLS to improve the solution, *i.e.*, by attempting to satisfy more XOR constraints. Eventually, FOURIERMAXSAT

achieved a relative score of 0.93.

Moreover, we observe that the instances for which FOURIERCSP attains the best solutions are typically those with larger problem sizes. This observation suggests a qualitative distinction in scalability: while systematic search solvers tend to be effective for smaller instances, FOURIERCSP exhibits improved scalability and maintains solution quality as instance size increases.

5. Conclusion and Future Directions

In this paper, we introduced FOURIERCSP, a novel continuous optimization framework for constraint satisfaction problems. By extending the Walsh-Fourier expansion to finite-domain variables, our approach can handle versatile constraints without the need for memory-intensive encodings or auxiliary variables. By randomized rounding, the discrete constraints are transformed into differentiable functions, enabling gradient-based optimization. We adopted multiple gradient-based approaches for our optimization framework, which are supported by theoretical guarantees on convergence. Empirical evaluations on benchmark suites demonstrated that FOURIERCSP is scalable and performs competitively. The experimental results indicate that FOURIERCSP is a substantial extension of FOURIERSAT, broadening the class of problems that can be efficiently solved using CLS techniques. Ultimately, the differentiable nature of FOURIERCSP facilitates seamless integration into neurosymbolic architectures, bridging the long-standing gap between data-driven deep learning and constraint reasoning.

The performance of Fourier transform-based CLS relies heavily on GPU parallelism. An important direction for future work is to investigate how this parallelism can be effectively leveraged when constraints exhibit non-structural patterns. One promising approach is to leverage compact symbolic data structures, such as decision diagrams, to represent constraints and compute their circuit-output probabilities efficiently (Appendix C). This would further generalize FOURIERCSP, enabling its application to a broader range of CSP problems.

Acknowledgments

We thank Moshe Vardi for the helpful and insightful comments and discussions that contributed to this work. This work was supported in part by the National Research Foundation under the Prime Minister’s Office, Singapore, through the Competitive Research Programme (project ID NRF-CRP24-2020-0002 and NRF-CRP24-2020-0003); in part by the Ministry of Education, Singapore, through the Academic Research Fund Tier 2 (project ID MOE-T2EP50221-0008); and in part by the National University of Singapore, through the Microelectronics Seed Fund (FY2024). Zhiwei Zhang is supported in part by NSF grants (IIS-1527668, CCF1704883, IIS1830549), DoD MURI grant (N00014-20-1-2787), Andrew Ladd Graduate Fellowship of Rice Ken Kennedy Institute, and an award from the Maryland Procurement Office.

References

- Aavani, A. Translating pseudo-boolean constraints into cnf. In *International Conference on Theory and Applications of Satisfiability Testing*, pp. 357–359. Springer, 2011.
- Alekhovich, M., Ben-Sasson, E., and Wigderson, A. Space complexity in propositional calculus. In *Proceedings of the thirty-second annual ACM symposium on Theory of computing*, pp. 358–367, 2000.
- Allen-Zhu, Z. and Orecchia, L. Linear coupling: An ultimate unification of gradient and mirror descent. *arXiv preprint arXiv:1407.1537*, 2014.
- Baluta, T., Shen, S., Shinde, S., Meel, K. S., and Saxena, P. Quantitative verification of neural networks and its security applications. In *Proceedings of the 2019 ACM SIGSAC Conference on Computer and Communications Security*, pp. 1249–1264, 2019.
- Blondel, M., Berthet, Q., Cuturi, M., Frostig, R., Hoyer, S., Llinares-López, F., Pedregosa, F., and Vert, J.-P. Efficient and modular implicit differentiation. *Advances in neural information processing systems*, 35:5230–5242, 2022.
- Bradbury, J., Frostig, R., Hawkins, P., Johnson, M. J., Leary, C., Maclaurin, D., Necula, G., Paszke, A., VanderPlas, J., Wanderman-Milne, S., and Zhang, Q. JAX: composable transformations of Python+NumPy programs, 2018. URL <http://github.com/google/jax>.
- Brailsford, S. C., Potts, C. N., and Smith, B. M. Constraint satisfaction problems: Algorithms and applications. *European journal of operational research*, 119(3):557–581, 1999.
- Bryant, R. E. Graph-based algorithms for boolean function manipulation. *Computers, IEEE Transactions on*, 100(8): 677–691, 1986.
- Bryant, R. E. Binary decision diagrams and beyond: Enabling technologies for formal verification. In *Proceedings of IEEE International Conference on Computer Aided Design (ICCAD)*, pp. 236–243. IEEE, 1995.
- Cen, Y., Zhang, Z., and Fong, X. Massively parallel continuous local search for hybrid sat solving on gpus. In *Proceedings of the AAAI Conference on Artificial Intelligence*, volume 39, pp. 11140–11149, 2025.
- Chen, Y. and Ye, X. Projection onto a simplex. *arXiv preprint arXiv:1101.6081*, 2011.
- Cheng, K. C. and Yap, R. H. An mdd-based generalized arc consistency algorithm for positive and negative table constraints and some global constraints. *Constraints*, 15(2):265–304, 2010.
- Crawford, J. M., Kearns, M. J., and Schapire, R. E. The minimal disagreement parity problem as a hard satisfiability problem. *Computational Intell. Research Lab and AT&T Bell Labs TR*, 1994.
- Elffers, J., Johannsen, J., Lauria, M., Magnard, T., Nordström, J., and Vinyals, M. Trade-offs between time and memory in a tighter model of cdcl sat solvers. In *Theory and Applications of Satisfiability Testing–SAT 2016: 19th International Conference, Bordeaux, France, July 5-8, 2016, Proceedings 19*, pp. 160–176. Springer, 2016.
- Gasse, M., Chételat, D., Ferroni, N., Charlin, L., and Lodi, A. Exact combinatorial optimization with graph convolutional neural networks. *Advances in neural information processing systems*, 32, 2019.
- Golia, P., Juba, B., and Meel, K. S. A scalable shannon entropy estimator. In *International Conference on Computer Aided Verification*, pp. 363–384. Springer, 2022.
- Goyal, K., Dumancic, S., and Blockeel, H. Deepsade: Learning neural networks that guarantee domain constraint satisfaction. In *Proceedings of the AAAI Conference on Artificial Intelligence*, volume 38, pp. 12199–12207, 2024.
- Gu, J. Global optimization for satisfiability (sat) problem. *IEEE Transactions on Knowledge and Data Engineering*, 6(3):361–381, 1994.
- Gurobi Optimization, LLC. Gurobi Optimizer Reference Manual, 2024. URL <https://www.gurobi.com>.
- Hebrard, E. Mistral, a constraint satisfaction library. *Proceedings of the Third International CSP Solver Competition*, 3(3):31–39, 2008.
- Ignatiev, A., Morgado, A., and Marques-Silva, J. Pysat: A python toolkit for prototyping with sat oracles. In

- International Conference on Theory and Applications of Satisfiability Testing*, pp. 428–437. Springer, 2018.
- Jain, P. and Kar, P. Non-convex optimization for machine learning. *arXiv preprint arXiv:1712.07897*, 2017.
- Khalil, E., Le Bodic, P., Song, L., Nemhauser, G., and Dilkina, B. Learning to branch in mixed integer programming. In *Proceedings of the AAAI conference on artificial intelligence*, volume 30, 2016.
- Kolaitis, P. G. and Vardi, M. Y. Conjunctive-query containment and constraint satisfaction. In *Proceedings of the seventeenth ACM SIGACT-SIGMOD-SIGART symposium on Principles of database systems*, pp. 205–213, 1998.
- Krupke, D., Lan, L., Perk, M., et al. The cp-sat primer: Using and understanding google or-tools’ cp-sat solver, 2024. URL <https://github.com/d-krupke/cpsat-primer>.
- Kuchcinski, K. and Szymanek, R. Jacop-java constraint programming solver. In *CP Solvers: Modeling, Applications, Integration, and Standardization, co-located with the 19th International Conference on Principles and Practice of Constraint Programming*, 2013.
- Kyrillidis, A., Shrivastava, A., Vardi, M., and Zhang, Z. Fouriersat: A fourier expansion-based algebraic framework for solving hybrid boolean constraints. In *Proceedings of the AAAI Conference on Artificial Intelligence*, volume 34, pp. 1552–1560, 2020.
- Kyrillidis, A., Shrivastava, A., Vardi, M. Y., and Zhang, Z. Solving hybrid boolean constraints in continuous space via multilinear fourier expansions. *Artificial Intelligence*, 299:103559, 2021a.
- Kyrillidis, A., Vardi, M., and Zhang, Z. On continuous local bdd-based search for hybrid sat solving. In *Proceedings of the AAAI Conference on Artificial Intelligence*, volume 35, pp. 3841–3850, 2021b.
- Li, C. M. Integrating equivalency reasoning into davis-putnam procedure. *AAAI/IAAI*, 2000:291–296, 2000.
- Lin, P., Zou, M., Chen, Z., and Cai, S. Parailp: A parallel local search framework for integer linear programming with cooperative evolution mechanism. In *Proceedings of the Thirty-Third International Joint Conference on Artificial Intelligence*, pp. 6949–6957, 2024.
- Ling, H., Wang, Z., and Wang, J. Learning to stop cut generation for efficient mixed-integer linear programming. In *Proceedings of the AAAI Conference on Artificial Intelligence*, volume 38, pp. 20759–20767, 2024.
- Miller, D. M. and Drechsler, R. Augmented sifting of multiple-valued decision diagrams. In *33rd International Symposium on Multiple-Valued Logic, 2003. Proceedings.*, pp. 375–382. IEEE, 2003.
- Nagy, S., Paredes, R., Dudek, J. M., Dueñas-Osorio, L., and Vardi, M. Y. Ising model partition-function computation as a weighted counting problem. *Physical Review E*, 109(5):055301, 2024.
- Nesterov, Y. *Introductory lectures on convex optimization: A basic course*, volume 87. Springer Science & Business Media, 2013.
- O’Donnell, R. *Analysis of boolean functions*. Cambridge University Press, 2014.
- Pearl, J. Belief updating by network propagation. In *Probabilistic Reasoning in Intelligent Systems*, pp. 143–237. Morgan Kaufmann San Francisco (CA), 1988.
- Perez, G. and Régin, J.-C. Efficient operations on mdds for building constraint programming models. In *IJCAI 2015*, 2015.
- Perron, L., Didier, F., and Gay, S. The cp-sat-lp solver. In Yap, R. H. C. (ed.), *29th International Conference on Principles and Practice of Constraint Programming (CP 2023)*, volume 280 of *Leibniz International Proceedings in Informatics (LIPIcs)*, pp. 3:1–3:2, Dagstuhl, Germany, 2023. Schloss Dagstuhl – Leibniz-Zentrum für Informatik. ISBN 978-3-95977-300-3. doi: 10.4230/LIPIcs.CP.2023.3. URL <https://drops.dagstuhl.de/opus/volltexte/2023/19040>.
- Pote, Y., Meel, K. S., and Yang, J. Towards real-time approximate counting. *Proceedings of the AAAI Conference on Artificial Intelligence*, 39(11):11318–11326, Apr. 2025. doi: 10.1609/aaai.v39i11.33231. URL <https://ojs.aaai.org/index.php/AAAI/article/view/33231>.
- Prud’homme, C. and Fages, J.-G. Choco-solver: A java library for constraint programming. *Journal of Open Source Software*, 7(78):4708, 2022. doi: 10.21105/joss.04708. URL <https://doi.org/10.21105/joss.04708>.
- Sasao, T., Fujita, M., et al. *Representations of discrete functions*. Springer, 1996.
- Schulte, C., Lagerkvist, M., and Tack, G. Gecode. *Software download and online material at the website: http://www.gecode.org*, pp. 11–13, 2006.
- Shafer, G. R. and Shenoy, P. P. Probability propagation. *Annals of mathematics and Artificial Intelligence*, 2:327–351, 1990.

- Thornton, M. and Nair, V. Efficient spectral coefficient calculation using circuit output probabilities. *Digital Signal Processing*, 4(4):245–254, 1994.
- Vardi, M. Y. and Zhang, Z. Quantum-inspired perfect matching under vertex-color constraints. *arXiv preprint arXiv:2209.13063*, 2022.
- Vo, T., Baiou, M., Nguyen, V. H., and Weng, P. Learning to cut generation in branch-and-cut algorithms for combinatorial optimization. *ACM Trans. Evol. Learn. Optim.*, 5(3), August 2025. ISSN 2688-299X. doi: 10.1145/3728371. URL <https://doi.org/10.1145/3728371>.
- Xu, H., Koenig, S., and Kumar, T. K. S. Towards effective deep learning for constraint satisfaction problems. In Hooker, J. (ed.), *Principles and Practice of Constraint Programming*, volume 11008 of *Lecture Notes in Computer Science*, pp. 588–597. Springer, 2018. doi: 10.1007/978-3-319-98334-9_38.
- Xu, Y., Li, W., Sanner, S., and Khalil, E. B. Self-supervised transformers as iterative solution improvers for constraint satisfaction. In *Forty-second International Conference on Machine Learning*, 2025. URL <https://openreview.net/forum?id=IQN6ID0snT>.
- Yang, J. and Meel, K. S. Engineering an efficient pb-xor solver. In *27th International Conference on Principles and Practice of Constraint Programming (CP 2021)*. Schloss-Dagstuhl-Leibniz Zentrum für Informatik, 2021.
- Zeng, S., Zhang, S., Li, S., Wu, F., and Li, X.-Y. Beyond local selection: Global cut selection for enhanced mixed-integer programming. *arXiv preprint arXiv:2503.15847*, 2025.
- Zhang, C., Gao, Y., and Nastos, J. Learning branching heuristics from graph neural networks. *arXiv preprint arXiv:2211.14405*, 2022.

A. Technical Proof

A.1. Proof of Theorem 3.4

Let $P \in \tilde{D}$ and $X \in D$.

$$\begin{aligned}
 \mathbb{E}_{X \sim \mathcal{S}_P} [\mathcal{F}(X)] &= \mathbb{E}_{X \sim \mathcal{S}_P} \left[\sum_{c \in C} f_c(X) \right] \\
 &= \sum_{c \in C} \mathbb{E}_{X \sim \mathcal{S}_P} [f_c(X)] \\
 &= \sum_{\alpha \in D} \hat{\mathcal{F}}(\alpha) \cdot \mathbb{E}_{X \sim \mathcal{S}_P} [\phi_\alpha(X)]
 \end{aligned} \tag{6}$$

Since $\phi_\alpha(X) \in \{0, 1\}$ By linearity of the expectation, we have

$$\begin{aligned}
 \mathbb{E}_{X \sim \mathcal{S}_P} [\phi_\alpha(X)] &= 1 \cdot \mathbb{P}_{X \sim \mathcal{S}_P} [\phi_\alpha(X) = 1] + 0 \cdot \mathbb{P}_{X \sim \mathcal{S}_P} [\phi_\alpha(X) = 0] \\
 &= \mathbb{P}_{X \sim \mathcal{S}_P} [\phi_\alpha(X) = 1] \\
 &= \mathbb{P}_{X \sim \mathcal{S}_P} \left[\prod_{i=1}^n \phi_{\alpha_i}(x_i) = 1 \right].
 \end{aligned} \tag{7}$$

As $\phi_{\alpha_i}(\cdot)$'s are indication function,

$$\begin{aligned}
 \mathbb{P}_{X \sim \mathcal{S}_P} \left[\prod_{i=1}^n \phi_{\alpha_i}(x_i) = 1 \right] &= \prod_{i=1}^n \mathbb{P}_{X \sim \mathcal{S}_P} [\phi_{\alpha_i}(x_i) = 1] \\
 &= \prod_{i=1}^n \mathbb{P}[\mathcal{R}(P)_i = x_i] \\
 &= \prod_{i=1}^n p_{i, x_i}
 \end{aligned} \tag{8}$$

where the second equation holds due to Definition 3.2. By substituting Eq. (7) and Eq. (8) into Eq. (6), we can have

$$\mathbb{E}_{X \sim \mathcal{S}_P} [\mathcal{F}(X)] = \sum_{\alpha \in D} \hat{\mathcal{F}}(\alpha) \cdot \prod_{i=1}^n p_{i, x_i}$$

A.2. Proof of Proposition 3.5

By the triangle inequality,

$$\begin{aligned}
 &|\mathcal{F}(P) - \mathcal{F}(P')| \\
 &\leq |\mathcal{F}(P_{1,1}, P_{1,2}, \dots, P_{n, |\text{dom}(x_n)|}) - \mathcal{F}(P'_{1,1}, P_{1,2}, \dots, P_{n, |\text{dom}(x_n)|})| \\
 &+ |\mathcal{F}(P'_{1,1}, P_{1,2}, \dots, y_{n, |\text{dom}(x_n)|}) - \mathcal{F}(P'_{1,1}, P'_{1,2}, \dots, P_{n, |\text{dom}(x_n)|})| + \dots \\
 &+ |\mathcal{F}(P'_{1,1}, P'_{1,2}, \dots, y_{n, |\text{dom}(x_n)|}) - \mathcal{F}(P'_{1,1}, P'_{1,2}, \dots, P'_{n, |\text{dom}(x_n)|})| \\
 &= |(P_{1,1} - P'_{1,1}) \cdot \partial_{1,1} \mathcal{F}(P'_{1,2}, \dots, P'_{n, |\text{dom}(x_n)|})| + \dots \\
 &+ |(P_{n, |\text{dom}(x_n)|} - P'_{n, |\text{dom}(x_n)|}) \cdot \partial_{n, |\text{dom}(x_n)|} \mathcal{F}(P'_{1,1}, \dots, P'_{n, |\text{dom}(x_n)|-1})|
 \end{aligned}$$

Since $\mathcal{F}(P)$ is a multilinear function, $|\partial_{i,j}\mathcal{F}| \leq |C|$ for all $i \in [n]$ and $j \in [|\text{dom}(x_i)|]$. Hence we have

$$\begin{aligned} & |(P_{1,1} - P'_{1,1})\partial_{1,1}\mathcal{F}(P_{1,2}, \dots, P_{n,|\text{dom}(x_n)|})| + \dots \\ & + |(P_{n,|\text{dom}(x_n)|} - P'_{n,|\text{dom}(x_n)|})\partial_{n,|\text{dom}(x_n)|}\mathcal{F}(P'_{1,1}, \dots, P'_{n,|\text{dom}(x_n)|-1})| \\ & \leq |C| \left(\sum_{i \in [n]} \sum_{j \in [|\text{dom}(x_i)|]} |P_{i,j} - P'_{i,j}| \right) \\ & \leq |C| \sqrt{N} \|P - P'\| \end{aligned}$$

The last inequality is an application of the Cauchy-Schwarz Inequality.

A.3. Proof of Theorem 3.6

- “ \Rightarrow ”: Suppose the Boolean formula F is satisfiable and $X \in D$ is one of the solutions. Then a real assignment $P \in \tilde{D}$ such that $\mathbb{P}(\mathcal{R}(P) = X) = 1$ we have $\mathbb{E}_{X \sim \mathcal{S}_P}[f_c(X)] = 1$ for $c \in C$. Therefore $\mathcal{F}(X) = |C|$ and $\max \mathbb{E}_{X \sim \mathcal{S}_P}[\mathcal{F}(X)] = |C|$.
- “ \Leftarrow ”: Suppose Eq. (2) holds. For every $c \in C$ we have $\mathbb{E}_{X \sim \mathcal{S}_P}[f_c(X)] = 1$. Thus, the rounding $X \sim \mathcal{S}_P$ is a discrete assignment that satisfies all constraints.

A.4. Proof of Lemma 3.7

Since \mathcal{F} is a multilinear function, it can be decomposed as

$$\mathcal{F}(P) = \sum_{j \in \text{dom}(x_1)} p_{1,j} g_j(P_{\setminus 1}) + h(P_{\setminus 1}),$$

where g_j 's and h are multilinear polynomials not depending on j . Let

$$\eta q_i = \begin{cases} \text{proj}_{\tilde{D}_i}(p_1 - \eta \nabla \mathcal{F}(p_1)) - p_1, & i = 1, \\ \vec{0}, & \text{otherwise,} \end{cases}$$

and ϵ be an arbitrary positive number. For all η such that $\eta \in (0, \epsilon)$, we have

$$\begin{aligned} & \mathcal{F}(P - \eta V) - \mathcal{F}(P) \\ & = \sum_{j \in \text{dom}(x_1)} \eta v_{1,j} \cdot g_j(P_{\setminus 1}) \\ & = \sum_{j \in \text{dom}(x_1)} (\text{proj}_{\tilde{D}}(p_1 - \eta \nabla \mathcal{F}(p_1))_j - p_{1,j}) \cdot g_j(P_{\setminus 1}). \end{aligned}$$

If $proj_{\Delta_1}(p_1 - \eta q_1)$ is on $\Delta \setminus \delta\Delta$, we have

$$\begin{aligned}
 & \frac{1}{\eta} (\mathcal{F}(P - \eta V) - \mathcal{F}(P)) \\
 &= \frac{1}{\eta} \sum_{j \in \text{dom}(x_1)} \left(\eta g_j(P_{\setminus 1}) - \frac{\sum_{j \in \text{dom}(x_1)} (p_{1,j} + \eta g_j(P_{\setminus 1})) - 1}{|\text{dom}(x_1)|} \right) g_j(P_{\setminus 1}) \\
 &= \sum_{j \in \text{dom}(x_1)} \left(g_j(P_{\setminus 1}) - \frac{\sum_{j \in \text{dom}(x_1)} g_j(P_{\setminus 1})}{|\text{dom}(x_1)|} \right) \cdot g_j(P_{\setminus 1}) \\
 &= \sum_{j \in \text{dom}(x_1)} g_j(P_{\setminus 1})^2 - \frac{1}{|\text{dom}(x_1)|} \left(\sum_{j \in \text{dom}(x_1)} g_j(P_{\setminus 1}) \right)^2 \\
 &= \left(\sum_{j \in \text{dom}(x_1)} g_j(P_{\setminus 1})^2 \right) \left(\sum_{j \in \text{dom}(x_1)} \frac{1}{|\text{dom}(x_1)|} \right) - \left(\sum_{j \in \text{dom}(x_1)} \frac{g_j(P_{\setminus 1})}{\sqrt{|\text{dom}(x_1)|}} \right)^2 \\
 &\geq 0
 \end{aligned}$$

The last inequality is the Cauchy-Schwarz inequality, where the equality holds when \mathcal{F} is a constant.

A.5. Proof of Theorem 3.8

From Lemma 3.7 we can observe that, if $proj_{\tilde{D}}(P - \eta V)$ is on $\delta\tilde{D}$, we can always find an $\epsilon' \in (0, \epsilon)$ such that for all $\eta' \in (0, \epsilon')$, $proj_{\tilde{D}}(P - \eta' V)$ is on $\tilde{D} \setminus \delta\tilde{D}$.

Lemma 3.7 states that, any interior point $a \in \tilde{D} \setminus \delta\tilde{D}$ cannot be a local maximum of $\mathcal{C}(a)$. In contrast, all local maxima must lie on the boundary $\delta\tilde{D}$. Hence, Lemma 3.7 directly results in Theorem 3.8.

A.6. Proof of Theorem 3.9

To prove Theorem 3.9, we first need to establish Lemma A.3. The proof of Lemma A.3 relies on three propositions.

Proposition A.1 (Projection Point (Nesterov, 2013)). *For $P, P' \in \tilde{D}$, let $h(P) = \|P - (P' + \eta \nabla \mathcal{F}(P'))\|^2$ and $P^* = \arg \min_{P \in \tilde{D}} h(P)$, we have*

$$\langle \nabla h(P^*), P - P^* \rangle \geq 0.$$

Note that the projection point P^* is $P' - \eta g(P')$; Hence, we have the following Proposition.

Proposition A.2 (Gradient Mapping (Kyrillidis et al., 2021a)). *Given a function \mathcal{F} defined on a convex set Ω , for every $P \in \Omega$, we have*

$$\langle \nabla \mathcal{F}(P), g(P) \rangle \geq \|g(P)\|^2,$$

where $g(P)$ is the gradient mapping.

Also, the proof relies on the consequence of Proposition 3.5. By representing $\nabla \mathcal{F}(y) - \nabla \mathcal{F}(z)$ as an integral, we have

$$\begin{aligned}
 & |\mathcal{F}(P) - \mathcal{F}(P') - \langle \nabla \mathcal{F}(P'), (P - P') \rangle| \\
 &= \left| \int_0^1 \langle \nabla \mathcal{F}(P' + t(P - P')), (P - P') \rangle dt - \langle \nabla \mathcal{F}(P'), (P - P') \rangle \right| \\
 &\leq \int_0^1 \|\nabla \mathcal{F}(P' + t(P - P')) - \nabla \mathcal{F}(P')\| \cdot \|P - P'\| dt \\
 &\leq \int_0^1 Lt \|P - P'\|^2 dt \\
 &= \frac{L}{2} \|P - P'\|^2 dt
 \end{aligned} \tag{9}$$

Lemma A.3. Let \mathcal{F} be a multilinear polynomial. Let n be the number of variable, then $N = \sum_{i=1}^n |\text{dom}(x_i)|$. Let $g(\cdot)$ be the projected gradient mapping onto the simplices \tilde{D} . Given $P, P' \in \tilde{D}$, if the step size satisfies $\eta \leq \frac{1}{L}$, then the projected gradient step $P = P' - \eta g(P')$ satisfies:

$$\mathcal{F}(P) - \mathcal{F}(P') \geq \frac{\eta}{2} \|g(P')\|^2$$

Proof of Lemma A.3. Eq. (9) can be rewritten as

$$\mathcal{F}(P) \leq \mathcal{C}(P') + \langle \nabla \mathcal{F}(P'), P - P' \rangle + \frac{L}{2} \|P - P'\|^2$$

Let $P = P' - \eta g(P')$, the above inequality becomes

$$\mathcal{F}(P) \leq \mathcal{F}(P') - \eta \langle \nabla \mathcal{F}(P'), g(P') \rangle + \frac{\eta^2 L}{2} \|g(P')\|^2.$$

Applying Proposition A.2 and let $\eta \leq \frac{1}{L}$, we then have

$$\begin{aligned} \mathcal{F}(P) &\leq \mathcal{F}(P') - \eta \|g(P')\|^2 + \frac{\eta}{2} \|g(P')\|^2 \\ &= \mathcal{F}(P') - \frac{\eta}{2} \|g(P')\|^2. \end{aligned}$$

□

From Lemma A.3, we can assume $\eta = \frac{1}{L}$. Consider a sequence of points P_t 's such that $P_{t+1} = P_t - \eta g(P_t)$. Due to Lemma A.3 we have $\mathcal{F}(P_{t+1}) - \mathcal{F}(P_t) \leq -\frac{\eta}{2} \|g(P_t)\|^2$. Given any initial point P_0 , it will converge to P^* . After T gradient steps, we have

$$\begin{aligned} \mathcal{F}(P^*) - \mathcal{F}(P_0) &\geq \frac{1}{2L} \sum_{t=0}^T \|g(P_t)\|^2 \\ &\geq \frac{T+1}{2L} \min_t \|g(P_t)\|^2, \end{aligned}$$

which can be rewritten as

$$\begin{aligned} \min_t \|g(P_t)\| &\leq \sqrt{\frac{2L}{T+1}} \sqrt{\mathcal{F}(P^*) - \mathcal{C}(P_0)} \\ &\leq \sqrt{\frac{2L}{T+1}} \sqrt{|C|} \end{aligned}$$

To achieve a point a_T such that $\|g(P_t)\| \leq \epsilon$, we require $\sqrt{\frac{2|C|L}{T+1}} \leq \epsilon$, which implies $T \sim \mathcal{O}\left(\frac{|C|L}{\epsilon^2}\right)$.

A.7. Proof of Theorem 3.10

We refer to the full convergence proof in Appendix B.2 of (Allen-Zhu & Orecchia, 2014). ρ was shown in Proposition 3.5 Here, we justify the expression of $\Theta = \sum_{i=1}^n \log |\text{dom}(x_i)|$ as the Bregman diameter under the negative-entropy potential, i.e., $\psi(P) = \langle P, \log P \rangle$. Hence the quantity Θ is defined as

$$\Theta = \sup_P (\psi(P) - \psi(P_0)),$$

where we choose P_0 to be the uniform distribution on each probability simplex, since this minimizes $\psi(P_0)$ and therefore yields the tightest bound. Hence,

$$\begin{aligned} \psi(P) &= \sum_{i=1}^n \sum_{j=1}^{|\text{dom}(x_i)|} p_{i,j} \log p_{i,j} \\ \psi(P_0) &= \sum_{i=1}^n \sum_{j=1}^{|\text{dom}(x_i)|} \frac{1}{|\text{dom}(x_i)|} \log \frac{1}{|\text{dom}(x_i)|} \end{aligned}$$

$$\begin{aligned}
 \Theta &= \sup_P (\psi(P) - \psi(P_0)) \\
 &= \max_P (\psi(P)) - \psi(P_0) \\
 &= \sum_{i=1}^n \max_{p_i} \left(\sum_{j=1}^{|\text{dom}(x_i)|} p_{i,j} \log p_{i,j} \right) + \sum_{i=1}^n \log |\text{dom}(x_i)| \\
 &= \sum_{i=1}^n \log |\text{dom}(x_i)|
 \end{aligned}$$

B. Benchmarks and Encodings

B.1. Task Scheduling Problem

Task scheduling problems can be useful in compilers for multi-core CPUs. Given a task graph $G(V, E)$, where $V \ni v$ is a set tasks, $E \ni (u \rightarrow v)$ is a set of task dependency. Given T clock cycles and S workers, we define variables $t_v \in \{0, \dots, T-1\}$ and $s_v \in \{0, \dots, S-1\}$ to denote the task v is execute at t_v by worker s_v . Then, the scheduling problem can be formulated as

$$\begin{aligned}
 F &= F_1 \wedge F_2, \\
 F_1 &= \bigwedge_{(u \rightarrow v) \in E} (t_u < t_v), \\
 F_2 &= \bigwedge_{(u \rightarrow v) \notin E} ((t_u \neq t_v) \vee (s_u \neq s_v)).
 \end{aligned}$$

For each $T \in \{32, 64, 128, 256, 512\}$, $S \in \{4, 8, 16\}$, we choose $|V| = T \cdot S/2$ to generate 10 directed graph $G(V, E)$. Every variable $v \in V$ has a variable index $idx(v)$. Between any two variable $u, v \in V$ and $idx(v) > idx(u)$, we add an edge $u \rightarrow v$ with probability $5^{idx(u) - idx(v)}$.

Circuit-Output Probability For any $(u \rightarrow v) \in E$, the corresponding Fourier expansion, *i.e.*, circuit-output probability of the constraint $c \in F_1$ can be written as

$$\begin{aligned}
 \mathbb{P}[t_u < t_v] &= 1 - \mathbb{P}[t_u \geq t_v] \\
 &= 1 - \sum_{i=0}^{T-1} \sum_{j=i+1}^{T-1} \mathbb{P}[t_u \geq i] \cdot \mathbb{P}[t_v = i],
 \end{aligned}$$

where $\mathbb{P}[t_u \geq i]$ can be efficiently computed by cumulative sum.

For any $(u \rightarrow v) \notin E$, the corresponding Fourier expansion, *i.e.*, circuit-output probability of the constraint $c \in F_2$ can be written as

$$\begin{aligned}
 \mathbb{P}[(t_u \neq t_v) \vee (s_u \neq s_v)] &= 1 - \mathbb{P}[(t_u = t_v) \wedge (s_u = s_v)] \\
 &= 1 - \mathbb{P}[(t_u = t_v)] \cdot \mathbb{P}[(s_u = s_v)].
 \end{aligned}$$

Linearization While encoding F_1 into ILP is straightforward, encoding F_2 requires auxiliary variables $q_{u,v,i} \in \{0, 1\}$.

$$\begin{aligned}
 F^{int} &= F_1^{int} \wedge F_2^{int} \wedge F_3^{int} \wedge F_4^{int} \wedge F_4^{int} \wedge F_6^{int}, \\
 F_1^{int} &= \bigwedge_{(u \rightarrow v) \in E} (t_v - t_u \geq 1), \\
 F_2^{int} &= \bigwedge_{(u \rightarrow v) \notin E} (t_u - t_v + Tq_{u,v,1} \geq 1), \\
 F_3^{int} &= \bigwedge_{(u \rightarrow v) \notin E} (t_v - t_u + Tq_{u,v,2} \geq 1), \\
 F_4^{int} &= \bigwedge_{(u \rightarrow v) \notin E} (s_u - s_v + Sq_{u,v,3} \geq 1), \\
 F_5^{int} &= \bigwedge_{(u \rightarrow v) \notin E} (s_v - s_u + Sq_{u,v,4} \geq 1), \\
 F_6^{int} &= \bigwedge_{(u \rightarrow v) \notin E} \left(\sum_{i=1}^4 q_{u,v,i} \leq 3 \right).
 \end{aligned}$$

For F_2^{int} to F_6^{int} , the interpretation is as follows: given $(u \rightarrow v) \notin E$, when $(t_u = t_v) \wedge (s_u = s_v)$, all $q_{u,v,i}$ should be 1 to satisfy the constraints in F_2^{int} to F_5^{int} . However, the constraint in F_6^{int} is violated. Only when $(t_u \neq t_v) \vee (s_u \neq s_v)$, at least one of the $q_{u,v,i}$ can be 0, then the constraint in F_6^{int} can be satisfied.

Booleanization To further Booleanize this problem into Boolean constraints, we use a log-2 encoding.

$$t_v = \sum_{i=0}^{\log_2(T)-1} 2^i t_{v,i}, \quad (10)$$

$$s_v = \sum_{i=0}^{\log_2(S)-1} 2^i s_{v,i}, \quad (11)$$

where $t_{v,i} \in \{0, 1\}$ and $s_{v,i} \in \{0, 1\}$. Similarly, substituting F_1^{int} with Eq. (10) directly leads to F_1^{bool} . And for encoding F_2 , we introduce $q_{u,v,i}^{(t)} \in \{0, 1\}$ and $q_{u,v,i}^{(s)} \in \{0, 1\}$.

$$\begin{aligned}
 F^{bool} &= F_1^{bool} \wedge F_2^{bool} \wedge F_3^{bool}, \\
 F_1^{bool} &= \bigwedge_{(u \rightarrow v) \in E} \left(\sum_{i=0}^{\log_2(T)-1} 2^i t_{v,i} - \sum_{i=0}^{\log_2(T)-1} 2^i t_{u,i} \geq 1 \right), \\
 F_2^{bool} &= \bigwedge_{(u \rightarrow v) \notin E} \bigwedge_{i=0}^{\log_2(T)-1} (t_{u,i} \oplus t_{v,i} \oplus \neg q_{u,v,i}^{(t)}), \\
 F_3^{bool} &= \bigwedge_{(u \rightarrow v) \notin E} \bigwedge_{i=0}^{\log_2(S)-1} (s_{u,i} \oplus s_{v,i} \oplus \neg q_{u,v,i}^{(s)}), \\
 F_4^{bool} &= \bigwedge_{(u \rightarrow v) \notin E} \left(\bigvee_{i=0}^{\log_2(T)-1} q_{u,v,i}^{(t)} \vee \bigvee_{i=0}^{\log_2(S)-1} q_{u,v,i}^{(s)} \right).
 \end{aligned}$$

F_2^{bool} and F_3^{bool} (resp. F_4^{bool}) should be interpreted similarly to F_2^{int} to F_5^{int} (resp. F_6^{int}). Any $t_{u,i} \neq t_{v,i}$ will lead to $q_{u,v,i}^{(t)} = 1$ (or s equivalently), the constraint in F_4^{bool} will be satisfied.

B.2. Graph Coloring Problem with Hashing Queries

Given a graph $G(V, E)$, where $V \ni v$ is a vertex set, $E \ni (u, v)$ is an edge set. Given C colors, we define variables $x_v \in \{0, \dots, C-1\}$ to denote the vertex v is colored by x_v .

Then, the graph coloring problem can be formulated as a constraint set

$$C_1 = \bigwedge_{(u,v) \in E} (x_u \neq x_v).$$

In this problem, we additionally use a hash function to generate soft modulo constraints. The hash code $h \in H$ randomly samples half of the variables from the vertex set. The hash function is defined by $\sum_{i \in h} x_i \pmod 2$. Then, the soft constraint set is:

$$C_2 = \bigwedge_{h \in H} \left(\sum_{i \in h} x_i \pmod 2 = 1 \right).$$

The constraint optimization problem is

$$\min_a |H| \cdot \text{cost}(C_1, a) + \text{cost}(C_2, a),$$

where $\text{cost}(C, a)$ is the number of unsatisfied constraints in C when given an assignment a .

For each $|V| \in \{512, 1024, 2048, 4096\}$, $C \in \{8, 16, 32, 64\}$, we generate 10 random regular graphs with degree $2C$. We add $|V|$ modulo constraints as soft constraints.

Circuit-Output Probability For any $(u, v) \in E$, the corresponding Fourier expansion, *i.e.*, circuit-output probability of the constraint $c \in C_1$ can be written as

$$\begin{aligned} \mathbb{P}[x_u \neq x_v] &= 1 - \mathbb{P}[x_u = x_v] \\ &= 1 - \mathbb{P}[x_u = i] \cdot \mathbb{P}[x_v = i]. \end{aligned}$$

For any $h \in H$, as inspired by the Fourier expansion of XOR constraints (Kyrillidis et al., 2020), the circuit-output probability of the constraint $c \in C_2$ can be written as

$$\begin{aligned} \mathbb{P} \left[\sum_{i \in h} x_i \pmod 2 = 1 \right] &= \mathbb{P}[x_j \pmod 2 = 0] \cdot \mathbb{P} \left[\sum_{i \in h \setminus j} x_i \pmod 2 = 1 \right] \\ &\quad + \mathbb{P}[x_j \pmod 2 = 1] \cdot \mathbb{P} \left[\sum_{i \in h \setminus j} x_i \pmod 2 = 0 \right] \\ &= \frac{1 - (1 - 2\mathbb{P}[x_j \pmod 2 = 1]) \cdot (1 - 2\mathbb{P} \left[\sum_{i \in h \setminus j} x_i \pmod 2 = 1 \right])}{2} \\ &= \frac{1 - \prod_{i \in h} \left(1 - 2 \sum_{j=0}^{\frac{C}{2}-1} \mathbb{P}[x_i = 2j + 1] \right)}{2}, \end{aligned}$$

which can be handled by slicing.

After the above relaxations, the main computation of FOURIERCSP can be amenable for parallelization using Jax (Bradbury et al., 2018).

Linearization When encoding C_1 for ILP, we introduce two auxiliary variables $q_{u,v}, q_{v,u} \in \{0, 1\}$ for every $(u, v) \in E$.

$$\begin{aligned} C_1^{int} &= \bigwedge_{(u,v) \in E} (x_u - x_v + Cq_{u,v} \geq 1), \\ C_2^{int} &= \bigwedge_{(u,v) \in E} (x_v - x_u + Cq_{v,u} \geq 1), \\ C_3^{int} &= \bigwedge_{(u,v) \in E} (q_{u,v} + q_{v,u} \leq 1). \end{aligned}$$

When encoding C_2 for ILP, we introduce two auxiliary variables $q_h \in \{0, \dots, \frac{|h|(C-1)}{2}\}$, and $p_h \in \{0, 1\}$ for every $h \in H$.

$$C_4^{int} = \bigwedge_{h \in H} \left(\sum_{i \in h} x_i - 2q_h + p_h = 0 \right),$$

where p_h should be 1 (resp. 0) when $\sum_{i \in h} x_i$ is odd (resp. even). Then ILP should be formulated as:

$$\begin{aligned} \min & |H| - \sum_{h \in H} p_h \\ \text{s.t.} & C_1^{int} \cup C_2^{int} \cup C_3^{int} \cup C_4^{int} \end{aligned}$$

Booleanization The Booleanization for PB-XOR is similar to the previous section.

$$x_v = \sum_{i=0}^{\log_2(C)-1} 2^i x_{v,i}, \quad (12)$$

where $x_{v,i} \in \{0, 1\}$.

For every $(u, v) \in E$, and $i \in \{0, \dots, \log_2(C) - 1\}$, we introduce an auxiliary variable $q_{u,v,i} \in \{0, 1\}$. Consequently, C_1 can be encoded by

$$\begin{aligned} C_1^{bool} &= \bigwedge_{(u,v) \in E} (x_{u,i} \oplus x_{v,i} \oplus \neg q_{u,v,i}), \\ C_2^{bool} &= \bigwedge_{(u,v) \in E} \left(\bigvee_{i=0}^{\log_2(C)-1} q_{u,v,i} \right). \end{aligned}$$

Note that the parity of x_u only depends on $x_{u,0}$. Hence, the soft constraint set C_2 can be encoded by

$$C_3^{bool} = \bigwedge_{h \in H} \left(\bigoplus_{i \in h} x_{i,0} \right)$$

Eventually, the constrained optimization problem becomes

$$\min_a |H| \cdot (\text{cost}(C_1^{bool}, a) + \text{cost}(C_2^{bool}, a)) + \text{cost}(C_3^{bool}, a).$$

C. Efficient Evaluation and Differentiation by Decision Diagrams

Theorem 3.6 reveals that CSP solving can be reduced to a continuous optimization problem. The performance of gradient-based optimization crucially depends on the efficiency of evaluating and differentiating the objective function. However, the complexity of evaluation and differentiation is in #P-hard, *i.e.*, Eq. (1) has at most exponentially many terms, in general. Motivated by (Thornton & Nair, 1994), we reformulate Eq. (1) to Circuit-Output Probability (COP), which admits more tractable computation when a structured representation can encode the underlying constraint, *i.e.*, decision diagrams.

Definition C.1 (Circuit-Output Probability). Let f_c be a discrete function over a set X of finite domain variables. Let P be the variable input probabilities. The circuit-output probability problem of f_c w.r.t P , denoted by $COP_c(P)$, is the probability of f_c outputs 1 given the value of each variable independently sampled from a multimodal distribution, i.e.,

$$COP_c(P) = \sum_{X \in D} f_c(X) \prod_{i=1}^n p_{i,x_i}.$$

Corollary C.2. Given a constraint c defined on a finite domain D , for a real point $P \in \tilde{D}$, we have

$$\mathbb{E}_{X \sim \mathcal{S}_P} [f_c(X)] = COP_c(P).$$

Proof of Corollary C.2. Let $P \in \tilde{D}$ and $X \in D$. For each $c \in C$, by linearity of expectation, we have

$$\begin{aligned} \mathbb{E}_{X \sim \mathcal{S}_P} [f_c(X)] &= 1 \cdot \mathbb{P}_{X \sim \mathcal{S}_P} [f_c(X) = 1] + 0 \cdot \mathbb{P}_{X \sim \mathcal{S}_P} [f_c(X) = 0] \\ &= \mathbb{P}_{X \sim \mathcal{S}_P} [f_c(X) = 1] \\ &= COP_c(P). \end{aligned}$$

□

Prior work demonstrates that BDD can encode many Boolean constraints in compact size (Kyriillidis et al., 2021b; Sasao et al., 1996; Aavani, 2011). The multiple-valued extension of BDD is called a multi-valued decision diagram (MDD) (Bryant, 1995). The MDD can be versatile in representing many constraints through the translation from table constraints (Cheng & Yap, 2010)¹. Similar to BDD, two MDDs can be combined through an APPLY operation (Bryant, 1986; Perez & Régin, 2015), offering flexibility in encoding versatile constraints. The MDDs can be reduced by merging nodes that have the same set of outgoing neighbors associated with the same label (Cheng & Yap, 2010; Perez & Régin, 2015). Moreover, the size can be further reduced by sifting (Miller & Drechsler, 2003). A compact-size decision diagram means that the COP on it can be evaluated and differentiated efficiently.

C.1. Evaluation

Lemma C.3 (Top-Down Evaluation). Let $G(V, E)$ be the MDD of constraint c , run Algorithm 2 on G with a real assignment $P \in \tilde{D}$. Let $X \in D$ randomly rounded from P by $\mathbb{P}[x_i = j] = p_{i,j}$ for all $j \in \text{dom}(x_i)$. For each $v \in V$, we have

$$m_{td}[v] = \mathbb{P}_{M,a}[v],$$

where $\mathbb{P}_{G,a}[v]$ is the probability that the node v is on the path generated by b on G . Especially,

$$m_{td}[\text{TRUE}] = COP_c(P_a),$$

i.e., Algorithm 2 returns the COP of G in time $O(|V|)$.

Proof of Lemma C.3. We prove by induction on the MDD $G(V, E)$. Let $A \in \tilde{D}$ and $B \in D$.

- *Basic step:* For the root node r of M , $m_{td}[r] = 1$. This equation holds because r is on the path generated by every discrete assignment on G .
- *Inductive step:* For each non-root node v of V , let $\text{par}_i(v)$ be the set of parent nodes of v with an edge labeled by i . After Algorithm 2 terminate, we have

$$m_{td}[v] = \sum_{u \in \text{par}_i(v)} a_{id(u),i} \cdot m_{td}[u],$$

¹A table constraint is explicitly represented as the set of solutions or non-solutions for that constraint.

Algorithm 2 Top-Down Traversal of MDD

Input An MDD $G(V, E)$ representation of constraint c , a real assignment $P \in \tilde{D}$.

Output Circuit-output probability $COP_c(P)$.

- 1: Let $m_{td}[v]$ be the forward message of each node $v \in V$, where the root node is initialized as 1, otherwise 0.
- 2: **for** $v \in \text{sorted}(V)$ **do**
- 3: **for** $u = \text{child}(v)$ **do**
- 4: $m_{td}[u] += p_{id(v), \text{label}(v,u)} \cdot m_{td}[v]$
- 5: **end for**
- 6: **end for**
- 7: **return** $m_{td}[\text{true}]$

where $id(u)$ is the mapping of the node u to the corresponding variable index. By inductive hypothesis,

$$\begin{aligned} m_{td}[v] &= \sum_{u \in \text{par}_i(v)} \mathbb{P}[b_{id(u)} = i] \cdot \mathbb{P}[u|G, A] \\ &= \mathbb{P}[v|G, A] \end{aligned}$$

The second equation holds because the events of reaching v from different parents are exclusive. □

Alternatively, traversing the MDD bottom-up can also compute the circuit-output probability.

Lemma C.4 (Bottom-Up Evaluation). *Let $G(V, E)$ be the MDD of constraint c , run Algorithm 2 on G with a real assignment $P \in \tilde{D}$. For each $v \in V$, let $f_{c,v}$ be the sub-function of the sub-MDD generated by regarding v as the root. The following holds:*

$$m_{bu}[v] = COP_{c,v}(P),$$

i.e., Algorithm 3 returns the COP of G and in time $O(|V|)$.

Proof of Lemma C.4. We prove this by structural induction on MDD $G(V, E)$. Let $A \in \tilde{D}$, we have

- *Basic step:* For the terminal nodes, $m_{bu}[\text{true}] = 1$ and $m_{bu}[\text{false}] = 0$. The statement holds since the sub-functions given by terminal nodes are constant functions with values 1 and 0, respectively.
- *Inductive step:* For each non-terminal node v , let $v.i$ be the child node connecting v by edge label i . after Algorithm 3 terminates, we have

$$m_{bu}[v] = \sum_{i \in \text{dom}(x_{id(v)})} a_{id(v), i} \cdot m_{bu}[v.i].$$

By the inductive hypothesis, we have

$$\begin{aligned} m_{bu}[v] &= \sum_{i=0}^k a_{id(v), i} \cdot COP_{c,v.i}(A) \\ &= \sum_{i=0}^k \mathbb{P}[b_{id(v)} = i] \cdot COP_{c,v.i}(A) \\ &= COP_{c,v}(A) \end{aligned}$$

where $COP_{c,v}$ denotes the circuit-output probability of subgraph of G rooted at node v . □

Algorithm 3 Bottom-Up Traversal of MDD

Input An MDD $G(V, E)$ representation of constraint c , a real assignment $P \in \tilde{D}$.

Output Circuit-output probability $COP_c(P)$.

- 1: Let $m_{bu}[v]$ be the bottom-up message of each node $v \in V$, where the true terminal node is initialized as 1, otherwise 0.
- 2: **for** $v \in \text{sorted}(V, \text{reverse}=\text{True})$ **do**
- 3: **for** $u \in \text{child}(v)$ **do**
- 4: $i = \text{id}(v)$
- 5: $m_{bu}[v]^+ = p_{\text{id}(v), \text{label}(v,u)} \cdot m_{bu}[u]$
- 6: **end for**
- 7: **end for**
- 8: **return** $m_{bu}[\text{root}]$

C.2. Differentiation

The main idea of differentiation is from probabilistic inference (Pearl, 1988; Shafer & Shenoy, 1990), which traverses the graph model top-down and bottom-up. The following theorem shows that the partial derivative of COP can be obtained by top-down and bottom-up messages from Algorithm 2 and 3.

Theorem C.5 (Derivatives). *After running Algorithm 2 and 3 on MDD for constraint c with a real assignment $P \in \tilde{D}$, the partial derivative of COP on $p_{i,j}$ for all $j \in \text{dom}(x_i)$ can be computed by*

$$\frac{\partial COP_c(P)}{\partial p_{i,j}} = \sum_{v \in \{u: \text{id}(u)=i\}} m_{td}[v] \cdot m_{bu}[v.j] \quad (13)$$

Proof of Theorem C.5. Given an MDD $G(V, E)$, expand all terminal nodes such that each can only have one parent node. The expanded MDD is called \mathcal{G} , which has a true terminal set T and a false terminal set F . We have the following by repeating the proof of Lemma C.3 and C.4 on \mathcal{G} .

$$COP_c(A) = \sum_{v \in T} \mathbb{P}[v|A, \mathcal{G}] = \sum_{v \in T} m'_{td}(v)$$

For any non-terminal node $v \notin (T \cup F)$,

$$\begin{aligned} m_{td}[v] &= m'_{td}[v], \\ m_{bu}[v] &= m'_{bu}[v]. \end{aligned}$$

For any true terminal node $v \in T$ and false terminal node $u \in F$,

$$\begin{aligned} m'_{bu}[v] &= 1, \\ m'_{bu}[u] &= 0. \end{aligned}$$

Now, we are ready to prove Theorem C.5.

$$\begin{aligned} COP_c(A) &= \mathbb{P}[f_c = 1|A, \mathcal{G}] \\ &= \sum_{v \in \{u: \text{id}(u)=i\}} \mathbb{P}[v|A, \mathcal{G}] \cdot \mathbb{P}[f_c = 1|v, A, \mathcal{G}] \\ &= \sum_{v \in \{u: \text{id}(u)=i\}} m'_{td}[v] \cdot m'_{bu}[v] \\ &= \sum_{v \in \{u: \text{id}(u)=i\}} m_{td}[v] \cdot m_{bu}[v] \\ &= \sum_{v \in \{u: \text{id}(u)=i\}} m_{td}[v] \cdot \sum_{j=0}^k a_{i,j} m_{bu}[v.j] \end{aligned}$$

Hence we have

$$\frac{\partial COP_c(P)}{\partial p_{i,j}} = \sum_{v \in \{u: id(u)=i\}} m_{td}[v] \cdot m_{bu}[v.j]$$

□

C.3. Parallel Decision Diagram Traversal

The decision diagram can be traversed in parallel. For example, MDDs can be represented as Listing 1 and Listing 2.

```

1 # vid, nid, eid, cid
2 1 1 0 5
3 1 1 1 2
4 1 1 2 5
5 2 2 0 5
6 2 2 1 3
7 2 2 2 5
8 3 3 0 5
9 3 3 1 4
10 3 3 2 5
11 4 4 0 5
12 4 4 1 6
13 4 4 2 5
14 0 0 0 0
15 0 0 0 0
16 0 0 0 0
    
```

Listing 1. $x_1 \wedge x_2 \wedge x_3 \wedge x_4$

```

1 # vid, nid, eid, cid
2 1 1 0 6
3 1 1 1 2
4 1 1 2 6
5 2 2 0 3
6 2 2 1 4
7 2 2 2 6
8 3 3 0 6
9 3 3 1 5
10 3 3 2 5
11 3 4 0 6
12 3 4 1 6
13 3 4 2 5
14 4 5 0 6
15 4 5 1 7
16 4 5 2 6
    
```

Listing 2. $x_1 \wedge (x_2 < x_3) \wedge x_4$

For every MDD, we call the kernel functions to traverse one edge at a time. The corresponding top-down and bottom-up message propagation kernels are shown in Listing 3 and Listing 4. To ensure uniform execution across threads, shorter MDD traces are padded with zeros. The kernel functions are designed to detect such padded entries (e.g., when `nid` equals zero) and skip message propagation accordingly.

```

1 __global__ void top_down_kernel(
2     const int* variable_id, const int* node_id, const int* edge_id, const int* child_id
3     ,
4     const float* p, const int* pointer_id, float* m_td
5 ) {
6     int idx = blockIdx.x * blockDim.x + threadIdx.x;
7     if (idx >= num_mdd) return;
    
```

```

8 |   int vid = variable_id[idx];
9 |   if (vid == 0) return;
10 |   int nid = node_id[idx];
11 |   int eid = edge_id[idx];
12 |   int cid = child_id[idx];
13 |   int pid = pointer_id[vid];
14 |
15 |   atomicAdd(&m_td[cid], m_td[nid] * p[pid + eid]);
16 | }

```

Listing 3. CUDA-style top-down message propagation kernel function

```

1 | __global__ void bottom_up_kernel(
2 |   const int* variable_id, const int* node_id, const int* edge_id, const int* child_id
3 |   ,
4 |   const float* p, const int* pointer_id, const int num_mdd, float* m_bu
5 | ) {
6 |   int idx = blockIdx.x * blockDim.x + threadIdx.x;
7 |   if (idx >= num_mdd) return;
8 |
9 |   int vid = variable_id[idx];
10 |  if (vid == 0) return;
11 |  int nid = node_id[idx];
12 |  int eid = edge_id[idx];
13 |  int cid = child_id[idx];
14 |  int pid = pointer_id[vid];
15 |
16 |  atomicAdd(&m_bu[nid], m_bu[cid] * p[pid + eid]);

```

Listing 4. CUDA-style bottom-up message propagation kernel function